Magnetic properties of mixed spinel BaTiO3-NiFe2O4 composites

Babusona Sarkar, Biswajit Dalal, Vishal Dev Ashok, Kaushik Chakrabarti, Amitava Mitra, and S. K. De

Articles you may be interested in

Study of 0.9 BaTiO3-0.1 Ni x Zn 1 − x Fe 2 O 4 magneto-electric composite ceramics
J. Appl. Phys. **113**, 114107 (2013); 10.1063/1.4796145

Investigation of structural, dielectric, and magnetic properties of hard and soft mixed ferrite composites
J. Appl. Phys. **112**, 054323 (2012); 10.1063/1.4752030

Magnetic and dielectric properties of sol-gel derived nanoparticles of double perovskite Y2NiMnO6
J. Appl. Phys. **112**, 044311 (2012); 10.1063/1.4748058

Study of electronic structure and magnetization correlations in hydrogenated and vacuum annealed Ni doped ZnO
J. Appl. Phys. **109**, 063907 (2011); 10.1063/1.3556458

Polarization relaxation mechanism of Ba 0.6 Sr 0.4 TiO 3 / Ni 0.8 Zn 0.2 Fe 2 O 4 composite with giant dielectric constant and high permeability
J. Appl. Phys. **108**, 074105 (2010); 10.1063/1.3490782

Magnetic properties of mixed spinel BaTiO$_3$-NiFe$_2$O$_4$ composites

Babusona Sarkar,[1] Biswajit Dalal,[1] Vishal Dev Ashok,[1] Kaushik Chakrabarti,[1] Amitava Mitra,[2] and S. K. De[1,a)]

[1]*Department of Materials Science, Indian Association for the Cultivation of Science, Jadavpur, Kolkata-700032, India*
[2]*Materials Science and Technology Division, CSIR-National Metallurgical Laboratory, Jamshedpur 831007, India*

Solid solution of nickel ferrite (NiFe$_2$O$_4$) and barium titanate (BaTiO$_3$), (100-x)BaTiO$_3$–(x) NiFe$_2$O$_4$ has been prepared by solid state reaction. Compressive strain is developed in NiFe$_2$O$_4$ due to mutual structural interaction across the interface of NiFe$_2$O$_4$ and BaTiO$_3$ phases. Quantitative analysis of X-ray diffraction and X-ray photo electron spectrum suggest mixed spinel structure of NiFe$_2$O$_4$. A systematic study of composition dependence of composite indicates BaTiO$_3$ causes a random distribution of Fe and Ni cations among octahedral and tetrahedral sites during non-equilibrium growth of NiFe$_2$O$_4$. The degree of inversion decreases monotonically from 0.97 to 0.75 with increase of BaTiO$_3$ content. Temperature dependence of magnetization has been analyzed by four sublattice model to describe complex magnetic exchange interactions in mixed spinel phase. Curie temperature and saturation magnetization decrease with increase of BaTiO$_3$ concentration. Enhancement of strain and larger occupancy of Ni^{2+} at tetrahedral site increase coercivity up to 200 Oe. Magnetostructual coupling induced by BaTiO$_3$ improves coercivity in NiFe$_2$O$_4$. An increase in the demagnetization and homogeneity in magnetization process in NiFe$_2$O$_4$ is observed due to the interaction with diamagnetic BaTiO$_3$. © 2014 AIP Publishing LLC.
[http://dx.doi.org/10.1063/1.4869782]

I. INTRODUCTION

Ferrite materials having the spinel structure are the magnetic materials with important electronic, structural, and magnetic properties. Spinel ferrites are the soft ferrimagnets having the general formula AB$_2$O$_4$ with two inequivalent cation lattice sites tetrahedral (T$_d$) and octahedral (O$_h$), where A is divalent cation and B is trivalent cation (Fe). In normal spinel structure, tetrahedral site is occupied by divalent cation, and octahedral site is occupied by trivalent cation. In inverse spinel configuration, tetrahedral site is fully occupied by half of trivalent atom (Fe^{3+}) and other half of trivalent atom (Fe^{3+}), and all divalent atom occupy the octahedral site. Nickel ferrite, NiFe$_2$O$_4$ (NFO), is a well known inverse spinel ferrite with high Curie temperature T$_C$ = 865 K. It exhibits the ferrimagnetism that originates from the antiparallel orientation of tetrahedral and octahedral site consisting of two magnetic sublattices. NFO is a very fascinating ferrimagnetic semiconductor with high spin polarisation which gives rise to novel applications in spin caloritronics and room temperature spin filtering devices.[1,2] Strength of magnetic exchange interaction is primarily dependent on the valence state of cation and also the chemical environment of cation.[3,4] Random cation distribution among tetrahedral and octahedral sites and oxidation state of cation strongly affect the magnetic behavior of ferrites.[5–8] Oxygen stoichiometry affects the valence state of Fe due to its more than one stable valence state and also controls the cation distribution among tetrahedral and octahedral sites.[9–12] The

degree of inversion, i.e., transformation from equilibrium inverse spinel to non-equilibrium normal spinel can be easily controlled by varying the preparation conditions and the materials combination.

Ferrimagnetic (FM)-ferroelectric (FE) composite constitutes an ideal interface which dominates both ferromagnetic and ferroelectric properties. Several factors such as intermixing between phases, pinning of ferromagnetic and ferroelectric domains, and transmission of strain between component phases play crucial roles to determine magnetic and electric properties of composite. Interfacial phenomena between FM and FE are mostly studied in epitaxial thin FM films grown on suitable FE substrates. Strain in thin films is introduced due to mismatch in crystal parameters and thermal expansion coefficient between the material and the substrate. Growth condition also controls the amount of strain in epitaxial films. Strain affects magnetic properties of ferrites significantly.[7,13,14] Strain mediated coupling between ferroelectric BaTiO$_3$ (BTO) and ferrimagnetic NFO modifies magnetic anisotropy of NFO film.[15] In epitaxial heterostructure, thin films of NFO are grown on crystal surface in which local symmetry and lattice parameter control the intrinsic property of NFO. Simultaneous growth of NFO and BTO in the same environment may affect the growth kinetics in NFO. Composites consisting of FM and FE phases are also very attractive and are very simple systems to engineer magnetic and electric properties through interfacial coupling among different degrees of freedom. Composite creates high density of interface which may lead to drastic modification of cation distribution in NFO. Synthesis of solid solution (100-x)BTO-(x)NFO is a very promising route to get an idea about mutual effects

---

a)Electronic mail: msskd@iacs.res.in

115, 123908-1

during the nucleation and growth process. Moreover, the complex nature of structural interface between BTO and NFO phases is not well understood. In this paper, our primary aim is to find the influence of BTO phase on the solidification process of NFO phase and to investigate magnetic properties of (100-x)BTO-(x)NFO solid solution.

II. EXPERIMENT

All the oxide chemicals were of analytical grade and were used without further purification. Solid solution (100-x)BTO-(x)NFO with x = 0, 20, 40, 50, 60, 80, and 100 were synthesized via a two step standard solid-state reaction method. At first, $BaCO_3$, TiO_2 on one hand and NiO, Fe_2O_3 on the other hand were taken separately in stoichiometric amount and mixed thoroughly in agate mortar. The mixtures were then calcined separately at 600 °C for 24 h. Second, stoichiometric amount of calcined powders were mixed thoroughly in order to create the (100-x)BTO-(x)NFO solid solution and then pressed in pellets using 7 tons of pressure. The pellets were then sintered at 1100 °C for 24 h in order to form well crystalline solid solution of BTO-NFO.

The crystalline phases of the samples were determined by high-resolution XPert PRO Panalytical X-ray diffractometer with Cu K_α radiation ($\lambda = 1.54$Å). X-ray diffraction (XRD) data were collected in the range of $2\theta = 15°$ to $70°$ in the steps of 0.02 with a duration of 6.0 s per step. The analysis of chemical states of the constituent atoms was performed from X-ray photoelectron spectroscopy (XPS) recorded with Omicron 0571 spectrometer using $MgK\alpha$, 1253.6 eV line, and spot size of 800 μm. Temperature dependent magnetization-magnetic field (M-H) measurements for all samples were carried out by Vibrating Sample Magnetometer (Cryo-genic Ltd., UK) from 300 K to 5 K and above room temperature by Vibrating Sample Magnetometer (Lakeshore 7404).

III. RESULTS AND DISCUSSION

A. Crystal Structure Characterization

The room temperature XRD patterns of (100-x)BTO-(x)NFO (x = 0, 20, 50, 80, 100) are shown in Fig. 1. The perovskite oxide BTO at room temperature has the tetragonal crystal structure whereas NFO is a cubic spinel. The diffraction peaks of pure BTO are indexed as (100), (110), (111), (002)/(200), (210), (211), (202)/(220). The characteristic
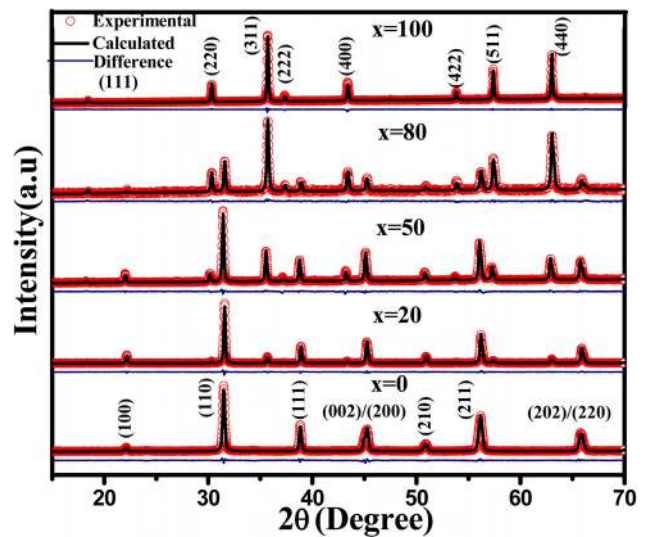

FIG. 1. Room temperature Rietveld fitted X- Ray diffraction pattern for x = 0, 20, 50, 80, and 100.

peaks of pure BTO are indexed as (111), (220), (311), (222), (400), (422), (511), (440). Absence of any other characteristic peak indicates the complete solid solution of a perovskite (BTO) and a spinel type oxide (NFO) for all samples. Structural refinements of the whole XRD pattern were carried out by Rietveld method using MAUD software[16] assuming space group P4/mmm for BTO and Fd3̄m for NFO. Peak profiles were fitted using psuedo-Voigt (pV) function with the background polynomial of order four. The reliability of analysis of XRD patterns depends on the residual factors R_{wp}, R_p, R_{exp}, and goodness of fit (GOF) parameter. The numerical values of all residual factors and GOF are shown in Table I. The structural parameters such as cell dimension, unit cell volume, atomic coordinates, occupation factor, and microstrain were refined during the fitting analysis.

The relative intensity of peaks for BTO diffractions increases with the increasing of BTO content. This suggests that BTO phase is incorporated into the NFO phase. The lattice parameter and unit cell volume of each phase are shown in Table I. BTO has a tetragonal unit cell with lattice parameters $a_{BTO} = 4.006$ Å, c = 4.017 Å, and NFO is the cubic spinel with lattice constant $a_{NFO} = 8.345$ Å. Unit cell volume of NFO decreases from 581.18 Å^3 to 578.25 Å^3, with increasing the BTO content which is attributed to the compressive strain

TABLE I. Parameters obtained from Rietveld refinement for BTO (Tetragonal (P4/mmm)) and NFO (Cubic (Fd3̄m)) phases. R_{wp} and R_p are the residual factors, and GOF is the goodness of fit parameter.

Composition	Weight (%)		Cell volume (Å^3)		Microstrain (%)		R_{wp}	R_p	GOF
	BTO	NFO	BTO	NFO	BTO	NFO			
x = 0	100		64.35		0.012		11.32	8.01	1.49
x = 20	81.08	18.92	64.23	578.25	0.010	0.105	7.61	5.40	1.31
x = 40	58.77	42.23	64.15	579.50	0.007	0.088	9.88	7.48	1.36
x = 50	52.68	47.32	64.09	579.88	0.006	0.072	7.26	5.40	1.39
x = 60	43.14	56.86	63.92	580.23	0.004	0.049	11.62	8.56	1.68
x = 80	25.63	74.37	63.85	580.80	0.001	0.031	12.02	8.87	1.39
x = 100		100		581.18		0.023	7.61	5.42	1.62

induced in the NFO lattice. Cell volume of BTO unit cell is increasing from 63.85 Å^3 to 64.35 Å^3, with the increasing of BTO content. Value of lattice parameter (a_{NFO}) of NFO is approximately twice of BTO lattice parameter (a_{BTO}). Percentage of microstrain is shown in Table I. The percentage of microstrain of both phases is increasing with the increasing of BTO content for the composites which may be attributed to the lattice mismatch of BTO and NFO. Decrease of unit cell volume of epitaxial thin film NFO grown on SrTiO$_3$ substrate is also observed and is consistent with the present result.[7,17] These observations indicate that the close proximity between NFO and BTO phases always creates compressive strain in NFO.

Cation arrangement of NFO was obtained by whole pattern fitting with use of Rietveld method.[3,6,18] The cation arrangement was obtained by refining the occupancy of individual cation at tetrahedral and octahedral sites. The cation distribution is quantified by the inversion parameter (δ) which denotes the fraction of divalent Ni^{2+} occupying octahedral site. The chemical formula based on inversion parameter is $[Ni_{1-\delta}^{2+}Fe_\delta^{3+}]_{Tetra}$ $[Ni_\delta^{2+}Fe_{2-\delta}^{3+}]_{Octa}O_4$. For fully inverse spinel, $\delta = 1$, and for normal spinel, $\delta = 0$. Details of occupancy and inversion parameter ($\delta = 1$) of each cation arrangement are shown in Table II. Inversion parameter (δ) for x = 100 is 0.97 as shown in Table II. Thus 3% Ni^{2+} ion goes to tetrahedral lattice site from octahedral coordination. Pure NFO has converted from inverse spinel to mixed spinel structure. Inversion parameter is gradually decreasing from 0.97 to 0.72 with increase of BTO content as displayed in Table II. In other words, the concentration of Ni^{2+} ion in the tetrahedral lattice site increases gradually from 3% to 28% for x = 80, 60, 50, 40, 20, i.e., with increase of BTO concentration. This suggests that BTO generates a driving force to move Ni^{2+} ion from the most preferable octahedral site of inverse spinel structure to tetrahedra sites of mixed spinel structure. The decrease of inversion parameter shows the increasing of mixed spinel structure. The reason for decrease of inversion parameter is the reduction of Fe-O and Ni-O bond from the octahedral lattice site. Oxygen atom can be easily removed from the octahedral site rather than the tetrahedral site due to the weak bond interactions of octahedral site.

B. X-Ray Photoelectron Spectroscopy

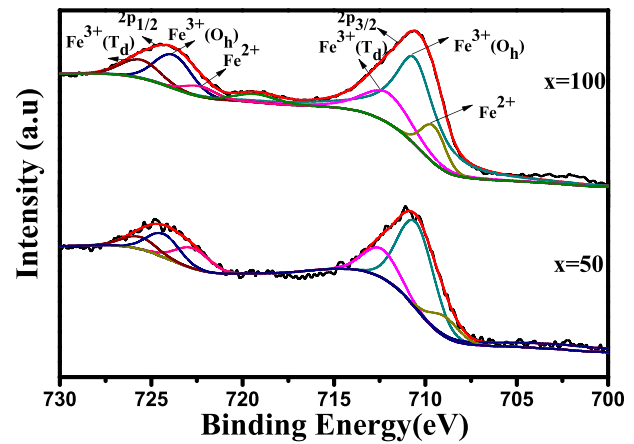High resolution X-ray photoelectron spectroscopy (HRXPS) was utilized to calculate the chemical environment

FIG. 2. Deconvolution of X-Ray Photoelectron spectra of Fe 2p$_{1/2}$ and 2p$_{3/2}$ region for x = 100 and x = 50.

and chemical state of cations, both qualitative and quantitative analysis. Core level XPS spectra for x = 100 and x = 50 were collected in 2 p region of Fe, and O 1s regions are shown in Figs. 2 and 3. The characteristics features and the energetic positions of peaks provide the evidence of cations at octahedral and tetrahedral sites.[9,12] The 2p peak region of both Ni and Fe are broader than the single Ni^{2+} and Fe^{3+} peaks that reveal that Ni and Fe are coordinated both octahedrally and tetrahedrally with oxygen. Spin-orbit interaction gives rise to splitting of 2p states into 2p$_{1/2}$ and 2p$_{3/2}$ levels as indicated in Fig. 2. For quantitative analysis, XPS spectra were deconvoluted using the Shirley type background correction. Deconvolution of Fe 2p spectra is resolved into three peaks, two of them are due to two lattice sites of Fe^{3+}, and third peak is for Fe^{2+} as indicated in Fig. 2. The binding energies associated with Fe^{3+}(O$_h$), Fe^{3+}(T$_d$), and Fe^{2+} of Fe2p$_{3/2}$ states are 710.75, 712.49, and 709.70 eV for x = 100 and 710.55, 712.12, and 709.10 eV for x = 50. The corresponding binding energies of Fe 2p$_{1/2}$ levels are 723.88, 725.94, and 722.67 eV for x = 100 and 723.70, 725.72, and 722.50 eV for x = 50. The lower binding energy of each spectrum belongs to Fe^{2+}. One satellite peak is observed for x = 100 around 719 eV due to Fe 2p$_{3/2}$ region. The appearance of peak corresponding to Fe^{2+} indicates the oxygen

TABLE II. Cation arrangement in Spinel NFO obtained from Rietveld refinement considering atomic coordinates of individual atom sites Ni(O$_h$)(x = y = z = 0.625), Fe(O$_h$)(x = y = z = 0.625), Ni(T$_d$)(x = y = z = 0), Fe(T$_d$)(x = y = z = 0), and O (x = y = z = 0.381). Occ and δ are the occupancy number of individual atom and inversion parameter, respectively.

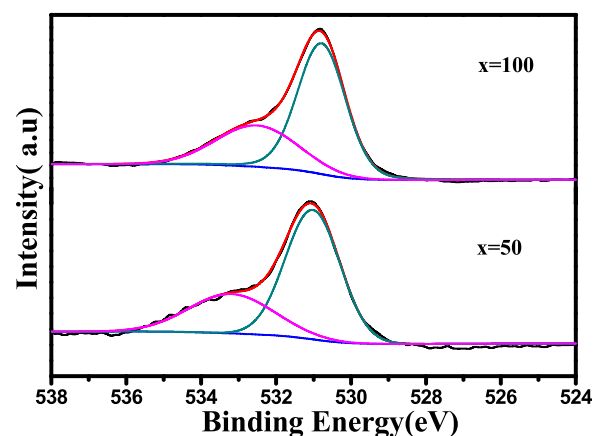|	x = 100	x = 80	x = 60	x = 50	x = 40	x = 20
atom site	Occ	Occ	Occ	Occ	Occ	Occ
Ni(O$_h$)	0.97	0.93	0.88	0.84	0.79	0.72
Fe(O$_h$)	1.03	1.07	1.12	1.16	1.21	1.28
Ni(T$_d$)	0.03	0.07	0.12	0.16	0.21	0.28
Fe(T$_d$)	0.97	0.93	0.88	0.84	0.79	0.72
δ	0.97	0.93	0.88	0.84	0.79	0.72

FIG. 3. Deconvolution of X-Ray Photoelectron spectra of O1s region for x = 100 and x = 50.

vacancy due to charge neutrality. The corresponding binding energy and integrated intensity in percentage of total area of Fe 2p spectra are shown in Table III. The contribution of $Fe^{3+}(T_d)$, $Fe^{3+}(O_h)$, and Fe^{2+} are 33%, 59%, and 8% for x = 100 and 27%, 61%, and 12% for x = 50 which are shown in Table III. Quantitative XPS analysis clearly indicates that the concentration of Fe^{3+} in tetrahedral site is decreased for x = 50 in comparison with x = 100.

Pure NFO is an inverse spinel in which all Ni^{2+} ions are octahedrally coordinated with oxygen. The percentage contribution of Ni^{2+} to octahedral and tetrahedral sites is shown in Table III. For x = 100, some (17%) Ni^{2+} tetrahedrally coordinated with oxygen proves the existence of mixed spinel in pure NFO. The binding energies as displayed in Table III corresponding to $Ni(O_h)$, and $Ni(T_d)$ of $Ni2p_{3/2}$ region are 855.20 and 856.63 eV for x = 100 and 855.11 and 856.47 eV for x = 50. The corresponding values of Ni $2p_{1/2}$ states are 872.78 and 874.67 eV for x = 100 and 872.69 and 874.58 eV for x = 50. The concentration of Ni^{2+} in tetrahedral site increases from 17% to 23% with decrease of x. This quantitative analysis strongly supports the increasing nature of mixed spinel phase with increasing of BTO content.

Oxygen vacancy is the most common defect of perovskite and spinel type oxide. Oxygen is more volatile than other constituent atoms of NFO. High temperature (1100 °C) synthesis of samples causes the release of oxygen from the oxides. The oxygen vacancies can be identified by carefully studying the XPS spectra. Oxygen 1s spectrum is very sensitive on the stoichiometric ratio. Core level O 1s spectrum is shown in Fig. 3 for x = 100 and x = 50. Deconvolution of O 1s spectra reveals the presence of two peaks at around 531.50 eV and 532.50 eV. Normally for oxide system, the lower binding energy peak corresponds to oxygen in intrinsical site, and higher binding energy peak is due to oxygen vacancy. The oxygen vacancy concentration (V_O) has been calculated from the integrated intensity. The value of V_O increases from 18% to 24% with increase of BTO concentration up to 50%. In spinel ferrite, oxygen can be easily removed from octahedral site due to the strong bond interaction of tetrahedral site. From XPS analysis, it is confirmed that reduced ionic state of Ni^{2+} does not exist in the sample. Reduction of Fe-O bond in octahedral site reduce the ionic state of Fe from Fe^{3+} to Fe^{2+}. Octahedral site preference energy of Fe^{3+}, Fe^{2+},

and Ni^{2+} is 0, 3.9, and 22.8 Kcal/mole.[19] Hence, the presence of Fe^{2+} in the system allows the possibility of Ni^{2+} ion occupying the tetrahedral site leading to a mixed spinel structure with a ratio of probabilities of 1:6 (i.e., for every 6 Fe^{2+} going to octahedral site will liberate enough energy to move one Ni^{2+} to go to tetrahedral site).

The most stable crystalline phase of NFO is inverse spinel which is energetically lower than normal spinel by 1.66 eV per formula unit based on self-interaction corrected local spin density approximation[20] and 1.78 eV per two formula unit based on generalized gradient approximation along with Hubbard correction.[4] Hence, a large amount of energy is generally required to modify cation distribution of the most stable inverse spinel phase. Experimentally, it is found that irradiation with fast neutrons of energy greater than 1 MeV can change the relative population of cation of inverse spinel phase.[21] High energy ball mill and high energetic ions in rf sputtering induce random distribution of cation.[7,8] Sintering temperature and rate of cooling also affects the cation distribution due to non-equilibrium thermodynamic condition.[22] Reduction of size promotes mixed spinel structure due to predominant surface effects.[23,24] Thus, external energy, synthesis procedure, and size can change the cation distribution. A slight deviation of cation distribution from inverse spinel phase of pure NFO may be due to high sintering temperature and cooling rate. NFO is surrounded by BTO phase during solidification. Sharing of thermal energy and the formation of interface between BTO and NFO phases may influence the nucleation and growth of NFO. BTO induces non-equilibrium growth condition of NFO phase which gives rise to movement of Ni^{2+} ion from O_h site to T_d site. The BTO phase reduces the energy barrier between inverse spinel and normal spinel phase. Thus, the degree of inversion decreases, i.e., the concentration of Ni^{2+} at tetrahedral site increases with increase of BTO phase.

C. Magnetization

Field cooled (FC) magnetization (M_{FC}) as a function of temperature for all samples is shown in Fig. 4 down to 5 K. The $M_{FC}(T)$ data show that ferrimagnetic transition occurs at about 848 K for pure NFO. The value of T_C decreases from 848 K to 836 K for solid solution with increase of BTO phase as depicted in Fig. 4(b) in enlarge view around transition temperature. The saturation magnetization in terms of mass of sample at low temperature shifts to lower value due to the presence of more non-magnetic BTO component in the solid solution. The temperature dependence of magnetization of normal spinel ferrimagnetic materials is conventionally explained by the theory proposed by Neel based on two-sublattice model.[25] The inverse spinel consists of two types of magnetic ions at octahedral (B) site, hence two sublattice model is not sufficient to interpret the magnetization data. Srivastava *et al.* proposed three sublattice model for inverse spinel to obtain correct magnetization because of the contribution of two magnetic ions in B site.[26] In mixed spinel structure, Fe and Ni atoms occupy both O_h and T_d sites. Here, we suggest a four sublattice model based on molecular field approximation due to extra contribution of Ni ion in

TABLE III. Energy (E) position and relative peak intensity of Fe 2 p and Ni 2 p region from X-ray photoelectron spectroscopy analysis.

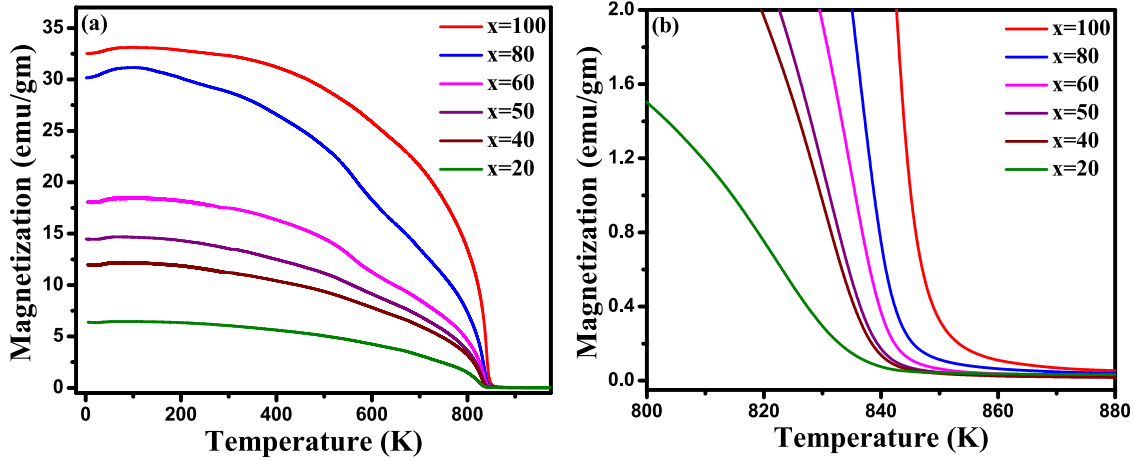| Sample	Lattice site	$E[2p_{3/2}]$(eV)	$E[2p_{1/2}]$(eV)	Peak intensity (%)
x = 100	$Fe^{3+}(O_h)$	710.75	723.88	59
	$Fe^{3+}(T_d)$	712.49	725.94	33
	Fe^{2+}	709.70	722.67	8
	$Ni^{2+}(O_h)$	855.20	872.78	83
	$Ni^{2+}(T_d)$	856.63	874.67	17
x = 50	$Fe^{3+}(O_h)$	710.55	723.70	61
	$Fe^{3+}(T_d)$	712.12	725.72	27
	Fe^{2+}	709.10	722.50	12
	$Ni^{2+}(O_h)$	855.11	872.69	67
	$Ni^{2+}(T_d)$	856.47	874.58	23

FIG. 4. (a) Field cooled magnetization vs temperature curve at magnetic field H = 1000 Oe for x = 20, 40, 50, 60, 80, and 100 and (b) enlarged view of magnetization vs temperature curve near Curie temperature for x = 20, 40, 50, 60, 80, and 100.

tetrahedral (A) site for mixed spinel. Hence, the occupancy of Fe and Ni in both octahedral and tetrahedral site constitute effectively four sublattice configuration. In the present model, Ni and Fe ions are aligned ferromagnetically in tetrahedral and octahedral lattices while are coupled antiferromagnetically between tetrahedral and octahedral sites. The net moment can be obtained by the sum of individual moment as described by following equations:

$$M_{total} = M_A + M_{A'} + M_B + M_{B'}, \qquad (1)$$

where $M_A, M_{A'}, M_B,$ and $M_{B'}$ are the magnetization contribution of Fe in tetrahedral site(Fe(T_d)), Ni in tetrahedral site(Ni(T_d)), Fe in octahedral site(Fe(O_h)), and Ni in octahedral site(Ni(O_h)), respectively. Individually, the sublattice magnetization M_i is given by

$$M_i = M_i(0)B_{S_i}(x_i), \quad i = A, A', B, B', \qquad (2)$$

where $M_i(0) = N_i g_i \mu_B S_i$, N_i is the number of magnetic ions per unit volume, g is the Lande g factor, and S_i is the moment of each magnetic ion (since for 3 d elements all the orbital angular moments are quenched) and $B_{S_i}(x_i)$ is the Brillouin function which is expressed as

$$B_{S_i}(x_i) = \frac{2S_i+1}{2S_i}\coth\left(\frac{2S_i+1}{2S_i}x_i\right) - \frac{1}{2S_i}\coth\left(\frac{x_i}{2S_i}\right). \quad (3)$$

x_i is obtained from the following relation:

$$x_i = \frac{g_i \mu_B S_i}{k_B T}\left(H - \sum_j \lambda_{ij}M_j\right), \quad (i,j) = A, A', B, B'(inorder).$$
$$(4)$$

H is the applied magnetic field which is taken as 1000 Oe. The sublattice magnetizations were determined by solving the four simultaneous self consistent equations.

The exchange constant (J_{ij}) is related to molecular field constant (λ_{ij}) as

$$J_{ij} = N_j g_i g_j \mu_B^2 \lambda_{ij}/2Z_{ij}. \qquad (5)$$

Z_{ij} is the number of nearest-neighbor of an atom on jth sub-lattice to an atom on ith sub-lattice. Crystallographic symmetry of inverse spinel and mixed spinel is identical except the cation distribution. Symmetry of mixed (inverse) spinel structure indicates that $Z_{ij} = 4$ for (i, j) = (A, A') and $Z_{ij} = 6$ for (i, j) = (B, B'). The coordination number of tetrahedral cation surrounded by octahedral cation (Z_{AB}, $Z_{A'B}$, $Z_{AB'}$ and $Z_{A'B'}$) is 12, whereas the coordination number of octahedral cation surrounded by tetrahedral cation (Z_{BA}, $Z_{BA'}$, $Z_{B'A}$ and $Z_{B'A'}$) is 6. The FC data are fitted to the magnetization obtained by solving the above equation using Levenberg Marquardt technique.

The best fitted magnetization data based on above equations for x = 100, 80, 50, 20 are displayed in Fig. 5. Individual cation and crystal site contributions to total magnetization are also indicated in Fig. 5. It is clear that contribution of magnetic ions in octahedral site is positive and larger whereas contribution of magnetic ions in tetrahedral site is negative and smaller. The overall behavior of individual magnetic component is consistent with theoretical prediction.[13,20,27] The calculated exchange constants (J) are shown in Table IV. The exchange interaction related to Ni(T_d)($J_{A'A'}$) is much weaker than the other interaction for x = 100 and gradually increases with for x = 80, 50, 20. Intersublattice ($J_{A'B'}$) and intrasublattice ($J_{A'A'}$ and $J_{B'B'}$) Ni-Ni exchange constants are positive, and all other exchange constants are negative as evident from Table IV. The corresponding values of intersublattice exchange interaction J_{AB}, $J_{A'B}$, $J_{AB'}$, and $J_{A'B'}$ are the half of J_{BA}, $J_{BA'}$, $J_{B'A}$, and $J_{B'A'}$. The negative J corresponds to ferromagnetic exchange interaction while positive J corresponds to antiferromagnetic exchange interaction as obvious from Eq. (4). It can be straight away observed that the intrasite (J_{AA} and J_{BB}) Fe-Fe are ferromagnetically coupled where as Ni-Ni are antiferromagnetically coupled. An increase in the octahedral contribution of Fe-Fe interaction is accompanied by a decrease in the tetrahedral contribution with a decrease in the composition of NFO. This is also accompanied with an increase in the antiferromagnetic intra site exchange in the tetrahedral Ni-Ni which is corroborated to the earlier observations if the exchange constants are considered to be a
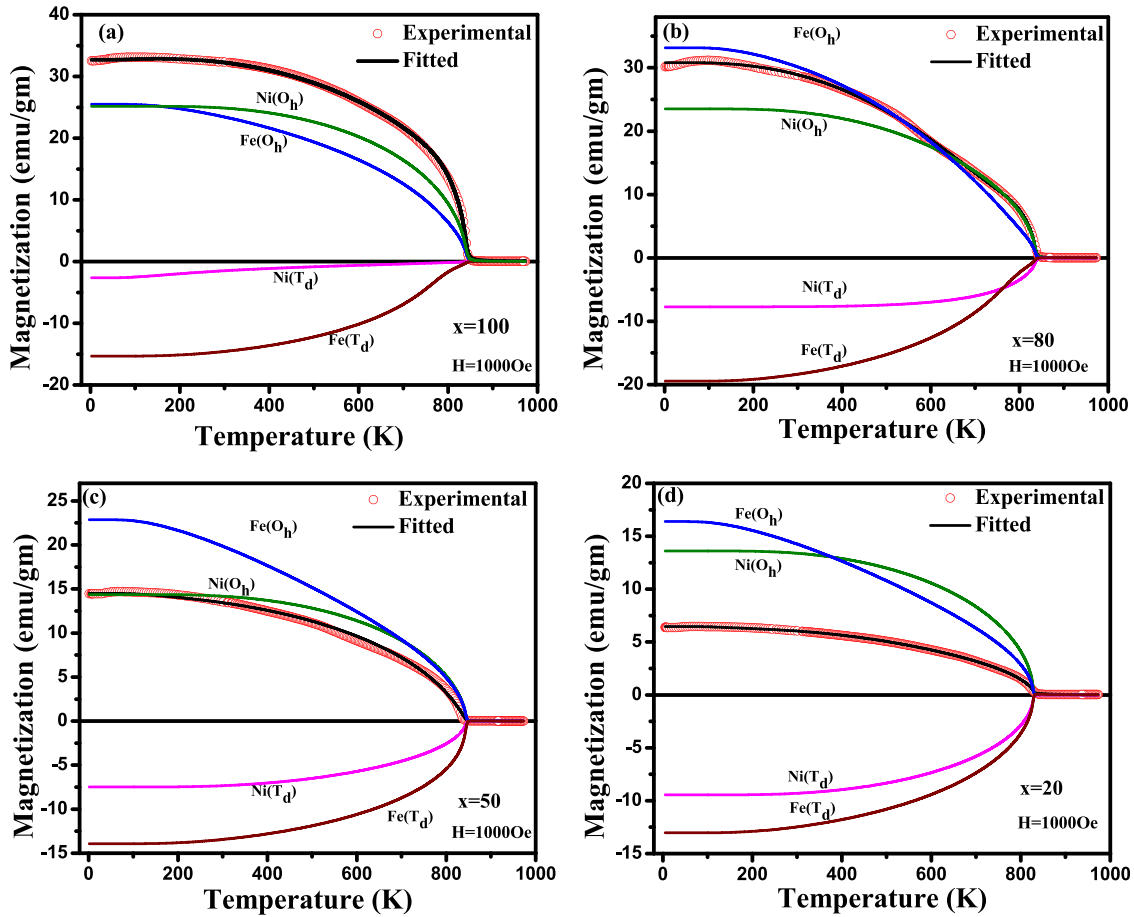
FIG. 5. Fitted magnetization vs temperature curve based on four sub lattice model for (a) x = 100, (b) x = 80, (c) x = 50, and (d) x = 20.

proportional to the number of orbital overlapping. Antiferromagnetic contribution is also seen in the case of intersite Ni-Ni exchange, which is observed to increase with an decrease in the content of NFO. All other intersite interactions seem to be ferromagnetic coupled which increase with decrease in the amount of NFO except when Ni in an octahedral site is coupled with an Fe, which leads to a decrease in the ferromagnetic interaction with a decrease in the composition. Antiferromagnetic contribution of Ni ions seems to decrease the net magnetization of the system with the decrease in the composition of NFO. The fitting results suggest that the rearrangement of Ni ions plays an important role in the overall magnetization of the composite.

Figure 6 shows the magnetization as a function of temperature in both zero field cooled (ZFC) and FC at an applied field of 1000 Oe for all compositions. The irreversible temperature (T_{irr}) between ZFC and FC process is found to be around 255 K for pure NFO. The ZFC magnetization

increases with decrease in temperature beyond T_{irr} showing a maximum around 145 K of temperature. The decreasing trend of ZFC magnetization below 145 K may be attributed to the random freezing of clusters into different metastable states.[28,29] The FC magnetization also shows a similar kind of behavior as observed in case of ZFC. The decrease in FC magnetization beyond the maximum may arise due to the strong antiferromagnetic inter-cluster interactions.[28] The T_{irr} temperature shifts above 300 K, and the difference between ZFC and FC curves increases with the decrease in x, i.e., increase of BTO. All the ZFC and FC curves show maxima similar to that observed for x = 100. The increase of T_{irr} above 300 K for x = 50 and 20 suggest that with the increase in BTO content in the solid solution it diffuses into the NFO during high temperature sintering, thereby hindering the motion of the domain wall of NFO with the application of the magnetic field thus increasing the T_{irr}.[30] The sample is cooled down in presence of a magnetic field which orient the

TABLE IV. Exchange constant (J_{ij}, in Kelvin) obtained from fitted data based on four sub-lattice model. J_{AB}, $J_{AB'}$, $J_{A'B}$, and $J_{A'B'}$ denote the intersublattice exchange interaction, and rest of all are the intrasublattice exchange interaction. A, A', B, and B' represent Fe(T_d), Ni(T_d), Fe(O_h), Ni(O_h), respectively.

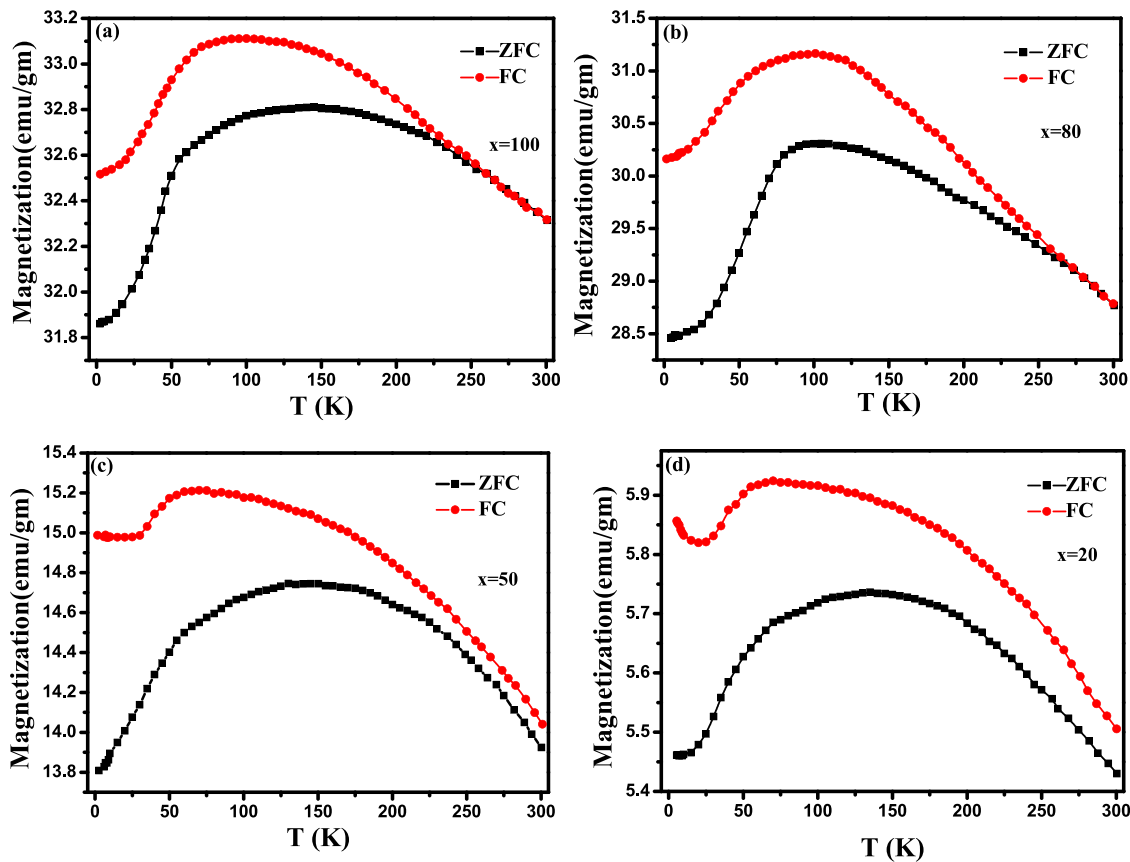| Composition	J_{AA}	$J_{AA'}$	$J_{A'A'}$	J_{AB}	$J_{AB'}$	$J_{A'B}$	$J_{A'B'}$	J_{BB}	$J_{BB'}$	$J_{B'B'}$
x = 100	−17	−1.83	1.54	−15.25	−11.39	−1.72	0.8	−3.4	−6.52	14
x = 80	−16	−2.07	3.22	−15.2	−10	−2	3.13	−5.2	−4.48	11.32
x = 50	−12	−3.61	5.37	−17.4	−9.18	−4.21	4.52	−6.5	−3.82	10
x = 20	−9	−4.9	5.9	−16	−9	−5.17	6.87	−6.8	−3.5	9

FIG. 6. ZFC and FC magnetization vs temperature curve below room temperature at magnetic field H = 1000 Oe for (a) x = 100, (b) x = 80, (c) x = 50, and (d) x = 20.

clusters along the field direction thereby reducing the antiferromagnetic interaction of the intercluster thus we obtain a large separation between the FC and ZFC curves below T_{irr}.[31] BTO is a purely diamagnetic oxide which always shields external magnetic field. An increase in the irreversible temperature is generally observed with a decrease in the applied magnetic field. Thus, the increase in the fraction of BTO in the composition, being diamagnetic in nature, leads to a decrease in the effective magnetic field observed by NFO resulting in the increase in T_{irr}.[9]

The magnetization-magnetic field (M-H) measurement at various temperatures is represented in Fig. 7. A saturation magnetization (M_S) is around 57.50 emu/gm at 5 K temperature as compared to reported bulk value of 55 emu/gm at the same temperature.[32] The 5% increase in M_S may be attributed to the cation distribution of NFO from well known inverse spinel type to a mixed spinel type. All the curves show thin hysteresis loop thus revealing a soft magnetic behavior due to the presence of NFO. The value of M_S decreases from 52.99 emu/gm(NFO) for x = 80 to 48.91 emu/gm(NFO) for x = 20, thus revealing the fact that M_S for the solid solution depends solely on the content of magnetic NFO phase only. The variation of M_S with x is shown in Fig. 8, thereby revealing the decreasing behavior of M_S with decrease in x.

Electronic configurations of Fe^{3+} and Ni^{2+} are $3d^5$ and $3d^8$, respectively. In high spin configuration, magnetic moments of Fe^{3+} and Ni^{2+} are 5 μ_B and 2 μ_B. In inverse spinel structure, first magnetic sublattice is ferromagnetically ordered Fe^{3+} ions

in tetrahedral site. Second sublattice consists of ferromagnetic ordered of Fe^{3+} and Ni^{2+} ions in octahedral site. Two sublattices are antiferromagnetically coupled and give rise to net magnetic moment of 2 μ_B per formula unit arising from purely Ni^{2+} ions. Theoretically, M_S should increase with decrease of inversion parameter. In the inverse spinel structure, Ni^{2+} moments in the octahedra site of the compound contributes to the net magnetization as Fe^{3+} moments from both tetrahedral and octahedral sites cancel each other due to antiferromagnetic ordering. The mixed spinel type on the other hand had some Ni^{2+} ions occupy the tetrahedral sites, resulting in an enhanced net magnetization as compared to inverse spinel type as the magnetic moment of Ni^{2+} at tetrahedral site is smaller compared to Fe^{3+} magnetic moment. The XRD analysis as described before reveals a 3% occupancy of Ni^{2+} ions at the tetrahedral site of the compound thereby increasing the value of M_S by 5%. The cation distribution from inverse spinel to mixed spinel type occurs mainly due to the missing oxygen bonds thereby weakening the effect of superexchange interactions.[9]

Figure 9 shows the dependence of coercivity (H_C) with the composition. The value of H_C increases from 50 Oe to 250 Oe with decrease of from x = 100 to 20. A sharp increase in H_C at x = 80 indicates a threshold concentration (20%) of BTO, which can significantly change the magnetization process. The shape of M-H curve depends on magnetic domain nucleation and growth process. The diffusion of BTO into NFO may happen at high temperature sintering and causes hindrance to the motion of NFO domain walls. The
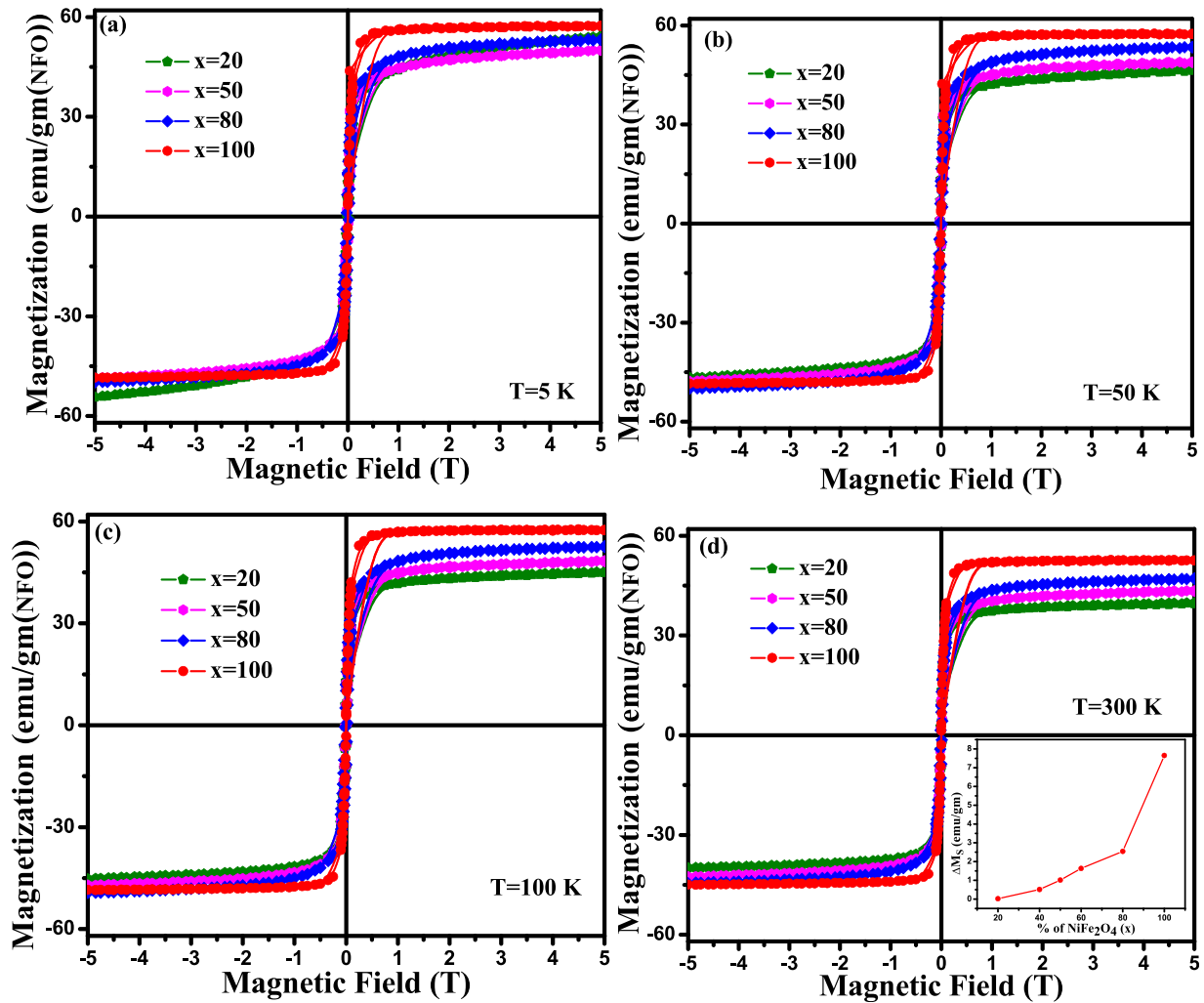
FIG. 7. Magnetization vs magnetic field hysteresis loop for x = 20, 50, 80, and 100 at temperature (a)T = 5 K, (b)T = 50 K, (c)T = 100 K, and (d)T = 300 K, and inset of (d) shows ΔM_S vs x at T = 300 K.

interpenetrating BTO may also inhibit domain nucleation and growth process. Domain growth is interrupted by defect created by oxygen vacancy. As a result of these, the increase of BTO phase enhances the value of H_C.[33]
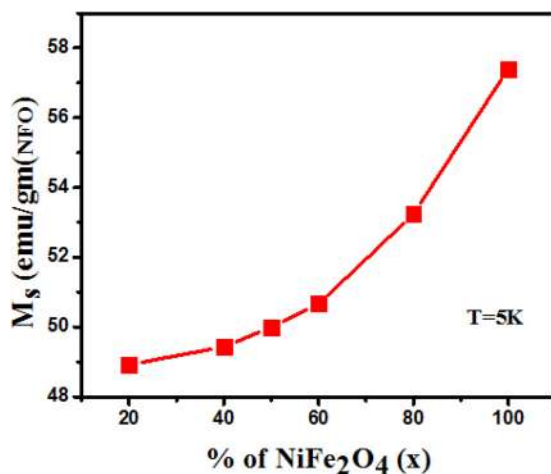
D. Magnetocrystalline anisotropy

Coercivity is determined by magneto crystalline anisotropy (MCA) which arises due to the spin-orbit coupling. Magnetic coercive field depends on magnetocrystalline anisotropy constant (K) by relationship, $H_c = \frac{2K}{M_S}$ as suggested
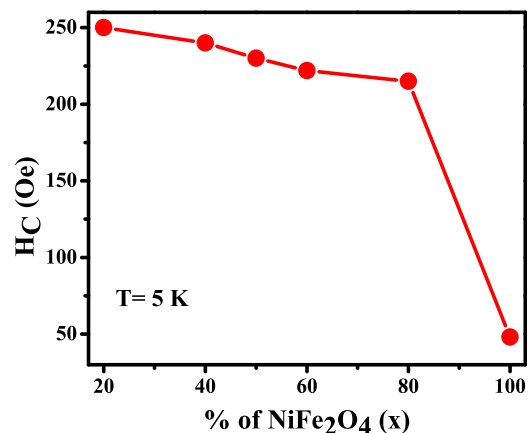

FIG. 8. Variation of saturation magnetization (M_S) with composition (x) at temperature T = 5 K.

FIG. 9. Variation of Coercivity (H_C) with composition (x) at temperature T = 5 K.

by Stoner–Wohlfarth model. In cubic magnetic structures like magnetic ferrites, K has low value and has low H_c. The strength of spin-orbit (S-O) interaction determines the magnitude of anisotropy energy. The ground state of Fe^{3+} ion is ^6S, i.e., angular moment is zero ($L = 0$). In a first order, perturbation of S-O effect gives rise to zero anisotropy energy. Thus the contribution of Fe^{3+} ion to anisotropy constant is small. The ground states of Ni^{2+} and Fe^{2+} are ^3F and ^5D, respectively. Ni^{2+} in tetrahedral site gives rise to larger anisotropy constant than that of octahedral site due to different orbital ground state.[34] The presence of Fe^{2+} also provides large contribution to anisotropy constant. Strain creates local distortion and introduces small perturbation in cubic symmetry. Theoretically, it is predicted that the compressive strain also enhances anisotropy energy.[35] The combined effect of inversion and strain enhance the value of H_c with increase of BTO content.

An asymmetry in saturation magnetization with the direction of applied magnetic field is observed in NFO as shown in Fig. 7. The difference in saturation magnetization $\Delta M_S = M_S(H_+)\text{-}M_S(H_-)$ where H_+ and H_- represents applied magnetic field in positive and negative direction, respectively, is shown in inset of Fig. 7(d). This difference in M_S gradually disappears with increase of BTO which implies that BTO plays an important role in magnetic field induced magnetization process of NFO. The shape of M-H curve primarily depends on magneto-crystalline anisotropy constants and demagnetizing factor (D). At lower field, the magnetization feature is composed of domain wall formation and growth bringing a complex nature to the M-H loop. Towards high field, the magnetization vs field curve may be approximated to a system consisting of freely rotating moment subjected to an anisotropy constant. Considering uniaxial symmetry, the behavior of these moments follow Stoner–Wohlfarth model given by[36]

$$\frac{2K_{eff}}{M_S} + \frac{4K_2}{M_S^3}M^2 - \frac{\mu_0 M_S H}{M} = 0, \quad (6)$$

where K_{eff} is the effective anisotropy consisting of the demagnetizing factor as given below

$$K_{eff} = K_1 + \frac{\mu_0 M_S^2(1 - 3D)}{4}, \quad (7)$$

where K_1 and K_2 represent the second and the fourth order uniaxial anisotropy and μ_0 is the free space permeability. Equation (6) suggests that the plot $\frac{H}{M}$ vs. M^2 yields a straight line whose intercept and slope provide K_{eff} and K_2. Two distinct values of K_{eff} are observed for the samples under positive and the negative magnetic field directions as shown in Fig. 10(a). The separation between the K_{eff} in the positive and the negative directions decreases exponentially with increase in the BTO composition as depicted in Fig. 10(b). This exponential nature leads us to believe that the discrepancy in this values of K_{eff} in positive and negative direction could be explained to arise due to a change in the demagnetization factor as evident from Eq. (7). The demagnetization factor is the ratio of the applied magnetic field to the
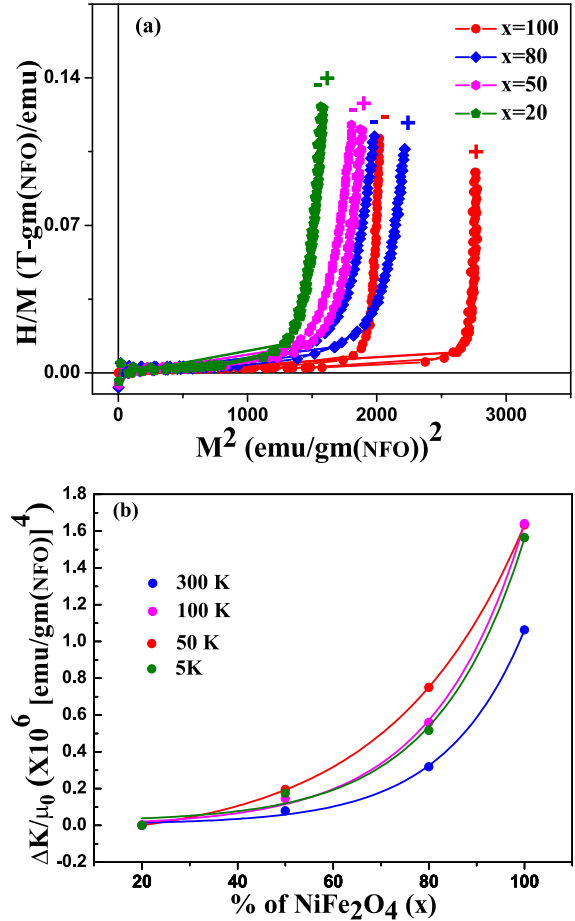

FIG. 10. (a) H/M vs M^2 plot for x = 20, 50, 80, and 100 at T = 300 K. The directions are indicated as + and − as parallel and anti parallel to the initially applied field respectively. and (b) difference in derived effective anisotropy constant (K_{eff}) vs composition (x).

magnetic field experienced by NFO. It is a signature of the shape of magnetic field inside the NFO phase due to the magnetic opacity of diamagnetic BTO. This is also corroborated by the increase in the T_{irr} of the system with an increase in BTO composition. In this sense, the magnetic properties of this system may be stated to vary from an inhomogeneous to a homogenous nature with the addition of BTO.

IV. CONCLUSION

Synthesis of (100-x)BTO-(x)NFO solid solution at high temperature stabilizes mixed spinel structure of NFO. The presence of BTO during the growth of NFO phase changes the cation distribution from inverse spinel to mixed spinel structure. Decrease of cell volume of NFO and increase of cell volume of BTO indicates a strong elastic coupling between two phases. Compressive strain in NFO may be due to non-equilibrium cation distribution which leads to mixed spinel structure. A dramatic increase in H_c for the composition ratio NFO:BTO:: 80:20 suggests that a critical concentration of BTO is required to influence magnetocrystalline anisotropy energy of NFO. The partial inversion of Ni^{2+} ions from octahedral sites to tetrahedral sites causes an enhancement of magnetocrystalline anisotropy which gives

rise to increase of coercive field with increase of BTO. The presence of diamagnetic BTO induces homogenous magnetization and decreases internal magnetic field of NFO. Strain mediated strong interaction between ferromagnetic order of NFO and ferroelectric order of BTO significantly modifies magnetic properties of NFO.

ACKNOWLEDGMENTS

[1]D. Meier, T. Kuschel, L. Shen, A. Gupta, T. Kikkawa, K. Uchida, E. Saitoh, J. M. Schmalhorst, and G. Reiss, Phys. Rev. B **87**, 054421 (2013).

[2]N. M. Caffrey, D. Fritsch, T. Archer, S. Sanvito, and C. Ederer, Phys. Rev. B **87**, 024419 (2013).

[3]Z. J. Zhang, Z. L. Wang, B. C. Chakoumakos, and J. S. Yin, J. Am. Chem. Soc. **120**, 1800 (1998).

[4]D. Fritsch and C. Ederer, Appl. Phys. Lett. **99**, 081916 (2011).

[5]A. Yang, Z. Chen, X. Zuo, D. Arena, J. Kirkland, C. Vittoria, and V. G. Harris, Appl. Phys. Lett. **86**, 252510 (2005).

[6]S. M. Patange, S. E. Shirsath, G. S. Jangam, K. S. Lohar, S. S. Jadhav, and K. M. Jadhav, J. Appl. Phys. **109**, 053909 (2011).

[7]U. Lüders, M. Bibes, J.-F. Bobo, M. Cantoni, R. Bertacco, and J. Fontcuberta, Phys. Rev. B **71**, 134419 (2005).

[8]C. N. Chinnasamy, A. Narayanasamy, N. Ponpandian, K. Chattopadhyay, K. Shinoda, B. Jeyadevan, K. Tohji, K. Nakatsuka, T. Furubayashi, and I. Nakatani, Phys. Rev. B **63**, 184108 (2001).

[9]G. H. Jaffari, A. K. Rumaiz, J. C. Woicik, and S. I. Shah, J. Appl. Phys. **111**, 093906 (2012).

[10]S. Anjum, G. H. Jaffari, A. K. Rumaiz, M. S. Rafique, and S. I. Shah, J. Phys. D: Appl. Phys. **43**, 265001 (2010).

[11]S. Ayyappan, S. P. Raja, C. Venkateswaran, J. Philip, and B. Raj, Appl. Phys. Lett. **96**, 143106 (2010).

[12]Z. Zhou, Y. Zhang, Z. Wang, W. Wei, W. Tang, J. Shi, and R. Xiong, Appl. Surf. Sci **254**, 6972 (2008).

[13]D. Fritsch and C. Ederer, Phys. Rev. B **82**, 104117 (2010).

[14]A. Lisfi, C. M. Williams, L. T. Nguyen, J. C. Lodder, A. Coleman, H. Corcoran, A. Johnson, P. Chang, A. Kumar, and W. Morgan, Phys. Rev. B **76**, 054405 (2007).

[15]R. V. Chopdekar, V. K. Malik, A. F. Rodrïguez, L. Le Guyader, Y. Takamura, A. Scholl, D. Stender, C. W. Schneider, C. Bernhard, F. Nolting, and L. J. Heyderman, Phys. Rev. B **86**, 014408 (2012).

[16]See http://www.ing.unitn.it/maud/S for information about MAUD version 2.046, 2006.

[17]S. Venzke, R. B. van Dover, J. M. Phillips, E. M. Gyorgy, T. Siegrist, C.-H. Chen, D. Werder, R. M. Fleming, R. J. Felder, E. Coleman, and R. Opila, J. Mater. Res. **11**, 1187 (1996).

[18]T. A. S. Ferreira, J. C. Waerenborgh, M. H. R. M. Mendonça, M. R. Nunes, and F. M. Costa, Solid State Sci. **5**, 383 (2003).

[19]D. S. McClure, J. Phys. Chem. Solids **3**, 311 (1957).

[20]Z. Szotek, W. M. Temmerman, D. Ködderitzsch, A. Svane, L. Petit, and H. Winter, Phys. Rev. B **74**, 174431 (2006).

[21]Yu. G. Chukalkin and V. R. Shtirts, Phys. Status Solidi A **160**, 185 (1997).

[22]J. M. Robertson and A. J. Pointon, Solid State Commun. **4**, 257 (1966).

[23]K. J. Kim, H. S. Lee, M. H. Lee, and S. H. Lee, J. Appl. Phys. **91**, 9974 (2002).

[24]Z. H. Zhou, J. M. Xue, J. Wang, H. S. O. Chan, T. Yu, and Z. X. Shen, J. Appl. Phys. **91**, 6015 (2002).

[25]L. Neel, Ann. Phys. **3**, 137 (1948).

[26]C. M. Srivastava, G. Srinivasan, and N. G. Nanadikar, Phys. Rev. B **19**, 499 (1979).

[27]H. Perron, T. Mellier, C. Domain, J. Roques, E. Simoni, R. Drot, and H. Catalette, J. Phys.: Condens. Matter **19**, 346219 (2007).

[28]D. Fiorani and S. Viticoli, J. Magn. Magn. Mater. **49**, 83 (1985).

[29]D. Fiorani, S. Viticoli, J. L. Dormann, J. L. Tholence, and A. P. Murani, Phys. Rev. B **30**, 2776 (1984).

[30]L. Lv, J. P. Zhou, G. Zhu, X. Z. Chen, X. B. Bian, and P. Liu, Physica E **43**, 1798 (2011).

[31]K. K. Bharathi, R. J. Tackett, C. E. Botez, and C. V. Ramana, J. Appl. Phys. **109**, 07A510 (2011).

[32]J. Smit and H. P. J. Wijn, *Ferrites* (Philips Technical Library, Eindhovan, The Netherlands, 1959), p. 157.

[33]J. P. Zhou, L. Lv, Q. Liu, Y. X. Zhang, and P. Liu, Sci. Technol. Adv. Mater. **13**, 045001 (2012).

[34]W. P. Wolf, Phys. Rev. **108**, 1152 (1957).

[35]H.-T. Jeng and G. Y. Guo, J. Magn. Magn. Mater. **240**, 436 (2002).

[36]E. C. Stoner and E. P. Wohlfarth, Philos. Trans. R. Soc. London A **240**, 599 (1948).